BASIC SCIENCE

Nanomedicine: Nanotechnology, Biology, and Medicine
14 (2018) 153–164

Original Article

nanomedjournal.com

A lithium-containing nanoporous coating on entangled titanium scaffold can enhance osseointegration through Wnt/β-catenin pathway

Wei Liu, PhD[a,1], Desheng Chen, PhD[c,1], Guofeng Jiang, PhD[b], Qiuyan Li, PhD[b], Qiaojie Wang, MD[a], Mengqi Cheng, PhD[a,*], Guo He, PhD[c,**], Xianlong Zhang, PhD[a,*]

[a]*Department of Orthopedic, Shanghai Jiao Tong University Affiliated Sixth People's Hospital, Shanghai, China*
[b]*State Key Lab of Metal Matrix Composites, School of Materials Science and Engineering, Shanghai Jiao Tong University, Shanghai, China*
[c]*Department of Orthopedic, General Hospital of NingxiaMedical University, Yinchuan, China*

Received 9 July 2017; accepted 15 September 2017

Abstract

An entangled titanium wire porous (ETP) scaffold shows similar mechanical properties of cancellous bone and is a promising bone repair material. However, the ETP scaffold's inert biocompatibility and poor osteogenic ability limit its clinical application. In this study, a Li-containing nanoporous coating was added on ETP by micro-arc oxidation (MAO). The SEM results indicated that a hierarchical and compact coating was formed on the Li-MAO-ETP scaffold. In vitro cell tests showed improved osteoblast morphology, adhesion, and viability in the Li-MAO-ETP group. Moreover, the Li-MAO-ETP scaffold exhibited improved osteogenic differentiation properties by activating the Wnt/β-catenin signal pathway based on the western blotting and RT-PCR results. The push-out test, sequential fluochrome labeling, and toluidine staining demonstrated that the Li-MAO-ETP scaffold contained improved osteogenic ability in vivo. The in vitro and in vivo experiments showed that the Li incorporated entangled porous titanium could be a suitable biomaterial for bone defect repair.
© 2017 Elsevier Inc. All rights reserved.

Key words: Entangled porous titanium; Lithium(li); Micro-arc oxidation; Wnt/β-catenin; Osteogenesis

Autologous bone, the current gold standard of bone grafts, is often used to treat bone defects in the clinic.[1] However, the elevated fracture rate, donor site morbidity, and lack of supply impede the extensive application of autologous bone.[2,3] Therefore, the development of bone graft substitutes is required. An ideal bone graft substitute should contain a similar elastic modulus to that of natural bone and exhibit a high fracture toughness. The mechanical support provided by traditional bone substitutes, such as ceramic-based or polymer-based scaffolds, often contains insufficient strength for bone repair at the load bearing site.[4,5] Based on our previous studies, the entangled titanium wire porous (ETP) scaffold could be an ideal bone substitute owing to its favorable mechanical properties (e.g., adequate toughness and high reliability in use) and interconnected porous structure.[6,7] Nevertheless, a long-term implantation outcome of the ETP scaffold should be further evaluated because of its suboptimal osseointegration ability, which may cause aseptic loosening and premature implant failure.

Therefore, to use the ETP scaffold for bone defect repair, the osteogenic ability and biocompatibility of the ETP scaffold should be enhanced to guarantee new bone growth when implanted in vivo. In recent years, surface modified technology has gained popularity because it can improve the microstructure and chemical composition of metal materials, while maintaining its mechanical properties. Specific methods have been employed to improve the biocompatibility of biomaterials, such as anodic oxidation, alkali heating, hydrothermal treatment, ion implantation, and micro-arc oxidation. Micro-arc oxidation (MAO), a convenient and effective wet-chemical method for regulating the elemental compositions and surface topographies by tailoring the components of the electrolytes,[8,9] was employed in this study. Because bone tissue is composed of microstructures, the nano-porous topographies created by MAO may provide a favorable environment for cell growth and cell–ECM interactions[10–12] Conversely, incorporating trace elements into

Funding: The present study was supported by Shanghai Jiao Tong University Medical-Engineering Crossing Foundation, China (grant no. YG2016MS14) and the National Natural Science Foundation of China (grant no. 81472109 and 81271962).

Conflict of interests: The authors declare no conflict of interest.

*Corresponding authors at: Xuhui District, Shanghai, CN 200233.
E-mail addresses: chengtu2006@126.com (M. Cheng), ghe@sjtu.edu.cn (G. He), dr_zhangxianlong@163.com (X. Zhang).

[1] Wei Liu and Desheng Chen contributed equally.

https://doi.org/10.1016/j.nano.2017.09.006
1549-9634/© 2017 Elsevier Inc. All rights reserved.

Please cite this article as: Liu W, et al, A lithium-containing nanoporous coating on entangled titanium scaffold can enhance osseointegration through Wnt/β-catenin pathway. *Nanomedicine: NBM* 2018;14:153-164, https://doi.org/10.1016/j.nano.2017.09.006

the MAO coatings will enhance the biological function of the coatings, which may stimulate osteoblast function and osseointegration.[13] However, only focusing on characteristics of materials or surface modified technology, leaving alone the related molecular mechanism or signal pathway for osteogenic differentiation and ECM mineralization would never fabricate an ideal bone repair material.

For the molecular mechanism of osteogenesis, several signal pathways are occupied in osteogenic differentiation and bone formation, and the Wnt/β-catenin pathway is important.[14] Generally, the Wnt/β-catenin pathway plays a vital role in embryonic development, cell proliferation, cell migration and tumorigenesis.[15] However, recent studies argued that the Wnt/β-catenin pathway was affected by local trace elements and implant surface topography that regulated several osteogenic processes ranging from osteoblast attachment and proliferation to differentiation and mineralization.[16–18] Furthermore, studies have demonstrated that the activation of the Wnt/β-catenin signal pathway may promote osteoblast proliferation and differentiation in vitro[19,20] and bone mineralization and formation in vivo.[21,22] However, the activity of this pathway is constitutively suppressed by glycogen synthase kinase-3β (GSK-3β).[23] The lithium (Li) ion, which can activate the canonical Wnt signal pathway by inhibiting GSK-3β,[24] has been proved to promote alkaline phosphatase and osteogenic genes expression in osteoblasts.[20,25] Oral administration of Li in mice can stimulate Wnt/β-catenin-mediated transcription in bone leading to an increase in bone mass and an improvement in fracture healing.[26,27] However, because Li is a non-selective GSK-3β inhibitor, systemic administration may induce severe adverse effects.[28] Thus, incorporating a significant amount of Li on the surface of the ETP scaffold to improve bone regeneration may be a suitable and effective way.

Previous studies have not evaluated an MAO method to incorporate Li on the surface of titanium or its scaffold. In this study, we introduced a Li-coating on the ETP scaffold to combine the advantages of the Li and MAO coatings, aiming to modulate the Wnt signal pathway and encourage bone formation. The objectives of this study were (1) to develop and characterize the Li-incorporated MAO coatings, (2) to determine whether the Li-incorporated MAO coatings could improve osseointegration, and (3) to investigate the underlying biological mechanism for the Li-incorporated MAO coatings on osseointegration.

Methods

Preparation and characterization of the Li-incorporated MAO coated ETP scaffold

A titanium wire with a diameter of 150 μm was used to fabricate the ETP scaffold using the filament winding method detailed in our previous study.[29] The yield strength and elastic modulus of the ETP scaffold were 17.7 ± 0.4 and 684.9 ± 6.6 MPa, respectively, when the porosity was 58.5 ± 0.2 and the pore size was 124 to 645 μm. Samples (Φ10 × 2 mm^2) were used for in vitro assays, and samples (Φ3 × 10 mm^2) were used for in vivo implantation. Lithium chloride (LiCl) was used as the Li source (Sigma-Aldrich). MAO was conducted in electrolytes composed of 0.04 mol/L NaH_2PO_4 and 0.1 mol/L $Ca(CH_3COO)_2$ to prepare the Li-free (L0-MAO) and Li-doped coatings (Lx-MAO). By adjusting the concentrations of LiCl (0.01 mol/L and 0.02 mol/L) in the electrolytes, the coatings designated as L1-MAO and L2-MAO were produced. During the MAO process, the applied voltage was 450 V, and the preparation time was 3 min. Field-emission scanning electron microscopy (FESEM, FEINOVA NanoSEM) was employed to observe the surface topography of the prepared specimens. The morphology of cross-section was also determined by SEM; the mechanical properties and pore size measurements were evaluated as our previous study.[29]

Ion release from the Li-incorporated MAO coating

The ETP scaffolds with various coatings were placed in sterile microcentrifuge tubes (15 ml) with 10 ml cell culture medium DMEM and incubated at 37 °C in a humidified atmosphere of 95% air and 5% CO_2 for 1, 3, and 7 days. At the end of each incubation period, extracts were collected. The concentrations of the Ca, P, and Li ions of the extracts were determined by ICP-MS (Inductively Coupled Plasma Mass Spectrometer, Thermo Scientific iCAP™ Q).

Observation of cell adhesion, spreading, and morphology

The human MG63 osteoblasts were cultured in Dulbecco's modified Eagle's medium (DMEM, Gibco) with 10% fetal bovine serum (Gibco) and 1% penicillin/streptomycin at 37 °C in a humid atmosphere of 5% CO_2. The culture medium was exchanged every 48 h. The MG-63 cells (1×10^4 cells/well) were cultured on the various coatings. After 1 and 4 days of incubation, the samples were washed twice with PBS, fixed in 4% paraformaldehyde for 15 min at room temperature, and permeabilized with 0.1% Triton X-100 for 2 min. For immunofluorescence imaging, the F-actin cytoskeleton of the osteoblasts was stained with phalloidin–rhodamine (Molecular Probes, Eugene, OR, USA) for 1 h, and the nuclei were counterstained with DAPI (Sigma, USA) for 15 min. Finally, the samples were imaged using a confocal microscope (Olympus Fluoview). SEM was applied to observe the cell morphology. The MG-63 cells were cultured on different coatings. After culturing for 4 days, the samples were washed with PBS and fixed in 2.5% glutaraldehyde at 4 °C for 2 h. Before the SEM observation, the samples were dehydrated with various concentrations of ethanol. Finally, the samples were sputtered coated with gold and observed with a field emission scanning electron microscope (FESEM, FEINOVA NanoSEM).

Cell proliferation and differentiation analysis

The MG-63 cells (1×10^4 cells/well) were seeded onto various coatings. After culturing for 1, 4, and 7 days, 20 μl of CCK-8 solution and 180 μl of culture medium were added to each well and then incubated for 2 h. Finally, the absorbance of the incubated solution was measured using a microplate reader at a 450-nm wavelength. Cell differentiation was assessed using an alkaline phosphatase (ALP) activity assay. The cells (1×10^4 cells/well) were cultured on various coatings for 7 and 14 days. At each time point, p-nitrophenyl phosphate (pNPP) (Sigma)

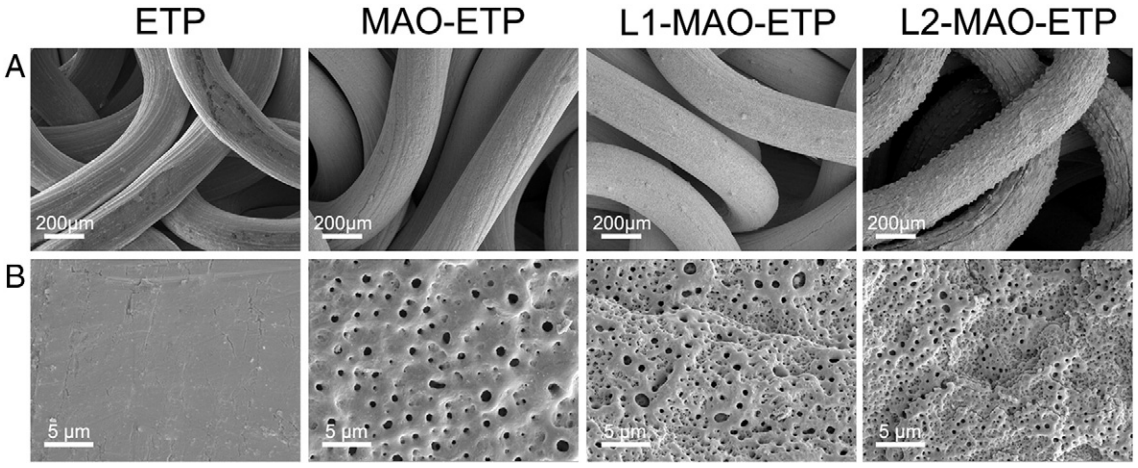

Figure 1. SEM images of the ETP, MAO-ETP, L1-MAO-ETP and L2-MAO-ETP scaffolds. The images in (**A**) are macroscopic image of the entangled titanium, and the (**B**) images are the surface nano-morphology of the entangled titanium.

was used as the reaction substrate, and the quantity of p-nitrophenol produced was measured at 405 nm. The total protein content was determined using the BCA Protein Assay Kit (Sigma), and the ALP activity was normalized by the total protein and expressed as nmol/min/mg protein.

Real-time polymerase chain reaction

Osteoblasts cultured on the scaffolds with different coatings were collected after incubation for 7 days to evaluate the osteogenesis-related gene expressions of Col1a1, ALP, OCN, OPN, and Runx2 as well as the Wnt/β-catenin signal related gene expressions of LRP5, LRP6, Axin 2, and β-catenin. The total RNA was extracted using a TRIzol reagent (Invitrogen). Subsequently, the complementary DNA (cDNA) was synthesized from 2 μg of total RNA using reverse transcriptase M-MLV (Takara). Quantifications of the selected genes were performed using real-time PCR with SYBR Premix Ex Taq (Takara). The primers used in this study are listed in Table S1, and β-actin was used as a housekeeping gene.

Western blotting

Lysates were extracted from the cultured osteoblasts using a mixture of T-PER Protein Extraction Reagent (Thermo Fisher Scientific), PhosSTOP (Roche, Basel, Switzerland), and cOmplete Mini (Roche). The protein samples were separated using 8% sodium dodecyl sulfate–polyacrylamide gel electrophoresis and were transferred to nitrocellulose membranes (Millipore, Billerica, USA). After blocking in phosphate-buffered saline/Tween-20 containing 5% non-fat milk, the membranes were incubated with the following primary antibodies: β-catenin (Santa Cruz Biotechnology, 1:100), β-catenin (pS37, Bioworld Technology, 1:100), GSK3-β (Abcam, 1:500), p-GSK3-β (Abcam, 1:500) or β-actin (Sigma-Aldrich, 1:20,000). The secondary antibody for β-catenin (pS37) and GSK3-β was anti-rabbit IgG (Sigma-Aldrich, 1:6000), and the secondary antibody for β-catenin and p-GSK3-β was anti-mouse IgG (Sigma-Aldrich, 1:5000). Subsequent visualization was performed with the SuperSignal West Femto Maximum Sensitivity Substrate (Thermo Fisher Scientific).

Animal experiment

The animal experiments were approved by the Animal Care Committee of Shanghai Sixth Hospital. Twenty-four adult male New Zealand white rabbits weighing 2.5 to 3.0 kg were used in the animal experiment. The rabbits were anesthetized by pentobarbital (25 mg/kg). After shaving and sterilization with iodophor disinfectant, the aspect of the femoral shaft was exposed. Then, two holes with a diameter of 3.0 mm were drilled, and the implants were pressed into the prepared holes. Finally, the subcutaneous tissue and skin were closed in various layers. The implants were placed bilaterally. Cefazolin (10 mg/kg) was injected into the muscle postoperatively for 3 consecutive days. After 12 weeks of implantation, the animals were euthanized, and the specimens containing the implants and surrounding bone tissue were harvested from the bilateral femurs for further examination.

Sequential fluorescent Labeling

At 4 and 8 weeks after the operation, alizarin red (30 mg/kg) and calcein (20 mg/kg) (Sigma) were injected into the rabbit intraperitoneally to label the newly formed bone. After 12 weeks of implantation, the scaffolds in the explanted femurs (n = 6 in each group) were collected and fixed in a neutral buffered formalin for 1 week. Then, the explanted femurs were dehydrated with ethanol and embedded in methyl methacrylate without decalcification. The nondecalcified sections were made on a saw microtome (Leica SP1600) and polished to a final thickness of approximately 50 μm. Then, the sections were observed using confocal laser scanning microscope (CLSM). Subsequently, the sections were stained with 1% methylene blue and measured using a digital image analysis system (Image-Pro Plus, Silver Spring, USA). The extent of bone ingrowth (ratio of bone tissue area to the implant pore area within the implant) was calculated based on toluidine blue staining.

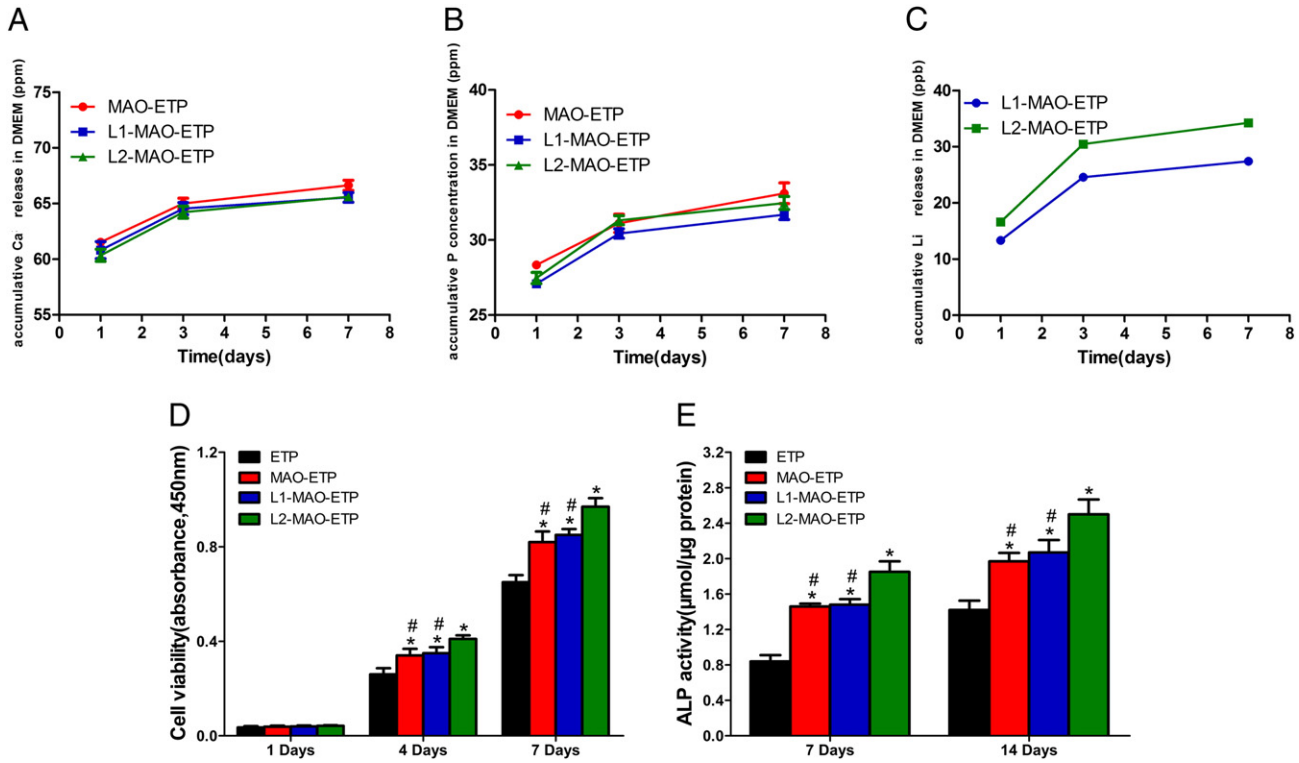

Figure 2. Ion concentrations of the ETP, MAO-ETP, L1-MAO-ETP and L2-MAO-ETP scaffolds immersed in a medium for 1, 3, and 7 days. The cell viability and ALP activity, (**A**) Li concentration, (**B**) Ca concentration, (**C**) P concentration, and (**D**) Cell viability of the osteoblasts were tested by CCK-8 at days 1, 4, and 7. The (**E**) ALP activity of the cells cultured on the entangled porous titanium at day 7 and 14. The symbols * and # represent $P < 0.05$ when compared with ETP and L2-MAO-ETP, respectively. A blank indicates no significant difference, $P > 0.05$).

Push-out test

Six samples in each group were harvested 12 weeks post-operation and fixed on a steel device with bone cement. The tests were performed at a loading rate of 1 mm/min. The load-deflection curves were recorded during the pushing period, and the failure load was defined as the maximum load.

Statistical analysis

The data were expressed as averages ± standard deviations. The results of the in vitro and in vivo experiments were statistically analyzed using one-way analysis of variance (ANOVA), and a P value less than 0.05 was considered to be statistically significant.

Results

Characterization of the Li-incorporated MAO coating

The SEM images of the ETP scaffolds with various surfaces are shown in Figure 1. The macroscopic images (Figure 1, *A*) show that the surface color changed from gray to white after Li was incorporated. The lithium oxide formed on the surface may be responsible for the color variation. The SEM images of the various coatings on the scaffolds are shown in Figure 1, *B*. A non-porous structure with minor scratches was visible on the uncoated ETP surface. After the MAO treatment, the coatings on the MAO-EPT ETP scaffold exhibited a nano-porous microstructure with homogeneously distributed micro-pores. Nevertheless, when a low concentration of LiCl (0.01 mol/L) was added to the electrolytes, the coatings on the L1-MAO-ETP displayed unconspicuous hierarchical micro-porous structures with increased porosity and surface roughness. Furthermore, when a high concentration of LiCl (0.02 mol/L) was added to the electrolytes, more obvious hierarchical nano-porous structures were formed on the L2-MAO-ETP scaffold, and the porosity, pore number, and surface roughness were increased. The hierarchical micro-porous structure and Li of the Li-MAO-ETP scaffold may enhance the performance of following in vitro and in vivo experiment. The cross-sectional morphology of the coating samples is shown in Figure S1. Figure S1 showed similar thickness of coatings about the three kinds of ETP. The average thickness of the coating was in the range of 4 to 6 μm; no significant difference was found on the thickness of coating among groups, which was consistent with some former studies on MAO coating.[11,30,31] The yield strength and elastic modulus of the coated ETP scaffold were at the range of 17.5 to 18.2 and 678.7 to 693.6 MPa; no significant difference was found among the groups, which demonstrated that the coatings on ETP scaffolds did not significantly influence the mechanical properties and pore size of ETP.

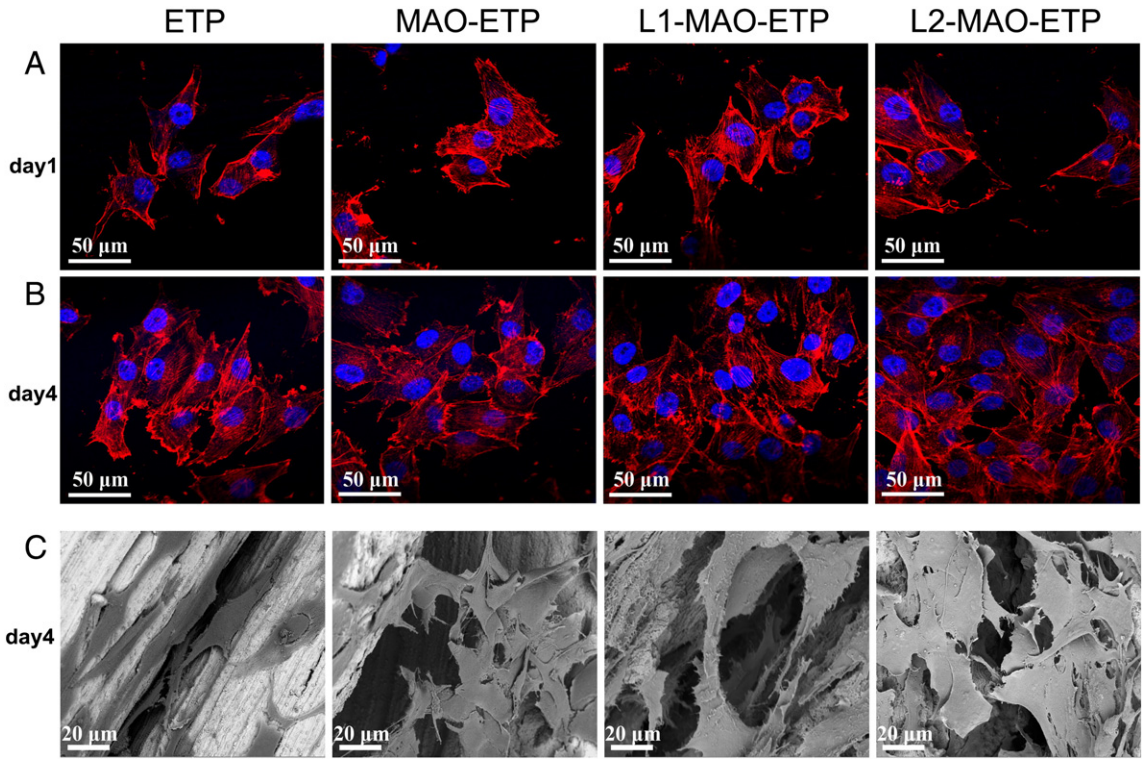

Figure 3. Cytoskeleton staining and cell adhesion on the entangled titanium. The images in (**A**) show the cell skeleton staining of the cells cultured on the materials at day 1. F-actin was stained red by rhodamine phalloidin, and nuclear was stained with blue by DAPI. The bar was 50 μm. The images in (**B**) are the cell skeleton staining at day 4, and (**C**) shows the SEM images of the cells cultured on the materials at day 4. The bar was 20 μm.

Ion release from the scaffolds

The scaffolds were immersed in DMEM for 1, 3, and 7 days. The concentrations of Ca, P, and Li were determined by ICP-MS. Larger amounts of Ca, P, and Li were released in the first 3 days. Then, the ion release rate slowed down (Figure 2, *A-C*). The Li-incorporated scaffolds released less Ca and P ions than the Li-free MAO scaffold (Figure 2, *A-B*). The Li concentration of the extracts for the Li-incorporated scaffolds was also determined. Figure 2, *C* shows that the L2-MAO-ETP scaffold released more Li ion than the L1-MAO-ETP scaffold when immersed in DMEM. The different release characteristics between the Li-free MAO and Li-incorporated scaffolds may be attributed to the hierarchical, compact surface coating on the Li-incorporated ETP scaffold.

Effect of the Li-incorporated MAO coating on cell adhesion and morphology

To investigate the cytoskeletal organization and cell density, osteoblasts on various surfaces were stained with Rhodamine–phalloidin and DAPI. As shown in Figure 3, *A* cells adhering to ETP, MAO-ETP, L1-MAO-ETP and L2-MAO-ETP were 6, 6, 7 and 7, respectively. The cell density and cytoskeletal organization on each sample contained a minimal change after incubation for 1 day. However, after incubation for 4 days, the osteoblasts on the L2-MAO-ETP scaffold displayed a high cell density and well-spread cytoskeletons. Cells adhering to ETP, MAO-ETP, L1-MAO-ETP and L2-MAO-ETP were 12, 16, 21 and 30, respectively, indicating that the L2-MAO coating provided a favorable environment for cell adhesion and growth (Figure 3, *B*). To further assess the interaction between the cells and various coatings, osteoblasts cultured on the coatings were observed by SEM. As shown in Figure 3, *C*, the filopodia of the cells on the L2-MAO coatings were more developed than those on other coatings. Furthermore, the mutual cross-linked cells on the L2-MAO coatings showed ingrowth behavior.

Effect of the Li-incorporated MAO coating on cell viability

The viability of the MG63 cells cultured for 1, 4, and 7 days on various scaffolds was evaluated by the CCK-8 assay (Figure 2, *D*). After incubation for 1 day, the cell viability of each sample contained no significant difference ($P > 0.05$). However, after incubation for 4 and 7 days, the cell viability of the L2-MAO-ETP scaffold was significantly higher ($P < 0.05$) than that of the other samples. Furthermore, there was no difference in the cell viability between the MAO-ETP and L1-MAO-ETP scaffolds. Therefore, the incorporation of an appropriate amount of Li into the MAO coatings on the ETP scaffold would be beneficial for osteoblast proliferation.

Effect of the Li-incorporated MAO coating on the ALP activity

As an early marker of the osteoblast differentiation, the ALP activity was measured at days 7 and 14 to investigate the osteogenic differentiation potential of MG63 cultured on the samples. As shown in Figure 2, *E*, the L2-MAO-ETP scaffold

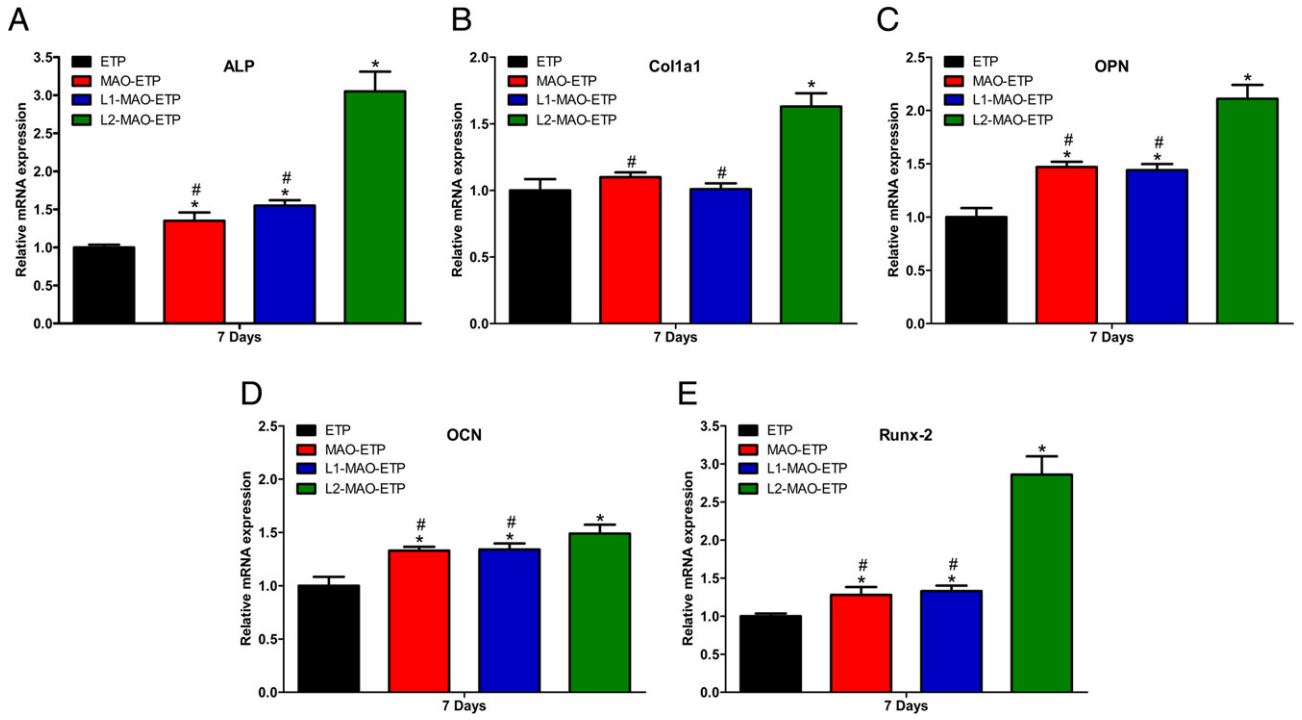

Figure 4. Osteogenesis-related gene expressions of the cells cultured on the entangled porous titanium for 7 days for (**A**) ALP, (**B**) COL1a1, (**C**) OPN, (**D**) OCN, and (**E**) RUNX-2. The symbols * and # represent $P < 0.05$ when compared with ETP and L2-MAO-ETP, respectively. A blank indicates no significant difference, $P > 0.05$.

displayed the highest ALP activity, and there was no statistical difference between the MAO-ETP and L1-MAO-ETP groups. Therefore, the ALP activity of MG63 on various coatings positively correlates with the Li amounts of the MAO coatings, and the L2-MAO coating increased the ALP activity in the early stage.

Effect of the Li-incorporated MAO coating on osteogenesis-related gene expressions

The expression of the osteogenic-related markers in the cells after incubation on the samples for 7 days was detected by a quantitative real-time polymerase chain reaction (qRT-PCR). The results were normalized to β-actin and expressed as relative expression levels to the uncoated ETP scaffold (Figure 4). Compared to uncoated ETP scaffold, the other scaffolds with different coatings promoted the expression of the tested genes. Furthermore, the expression levels for ALP, OPN, OCN, Col1a1, and Runx2 in the MG63 cells cultured on the L2-MAO coatings were higher than those on the MAO and L1-MAO coatings ($P < 0.05$). Therefore, the L2-MAO coating provided the greatest cell differentiation. However, no significant difference was observed between the MAO and L1-MAO coatings; thus, the low amount of Li incorporated into the MAO coatings was insufficient to promote osteogenic gene expression.

Effect of the Li-incorporated MAO coating on the Wnt signal pathway

The expressions of the Wnt/β-catenin pathway modulators were monitored by real-time PCR. After 7 days of incubation, the expression levels of LRP5 and LRP6 in the MG63 culture on the L2-MAO coatings were higher than those on the MAO and L1-MAO coatings ($P < 0.05$) (Figure 5, *A-B*), while no significant changes were observed ($P > 0.05$) between the MAO and L1-MAO coatings (Figure 5, *A-B*). For Axin2, the expression levels were significantly greater on the L1-MAO and L2-MAO coatings than those on the ETP and MAO-ETP scaffolds ($P < 0.05$) (Figure 5, *C*). β-Catenin, the core protein of the Wnt/β-catenin signal pathway, was further examined by a western blot after 7 days of incubation. As shown in Figure 5, *E* and the gene expression shown in Figure 5, *D*, the L2-MAO coatings showed the highest β-catenin levels, while no significant difference were observed between the MAO and L1-MAO coatings (Figure 5, *F*). In addition, the L2-MAO coatings decreased the amount of phosphorylated β-catenin. Thus, the L2-MAO coatings activated the β-catenin signal by up-regulating the expression of β-catenin and reducing the phosphorylation of β-catenin. Moreover, we also investigated the expression of GSK-3β through western blotting. Figure S2 showed that less activated p-GSK-3β was observed in Li containing ETP groups than ETP or MAO-ETP group, which indicated that the activity of GSK-3β was inhibited by Li.

Effect of the Li-incorporated MAO coating on in vivo osseointegration

After 12 weeks, push-out experiments (Figure 6, *A*) were performed to analyze the interfacial binding capacity between the implants and bone tissues. The average push-out loads and typical load-deflection curves are shown in Figure 6, *B-C*. The

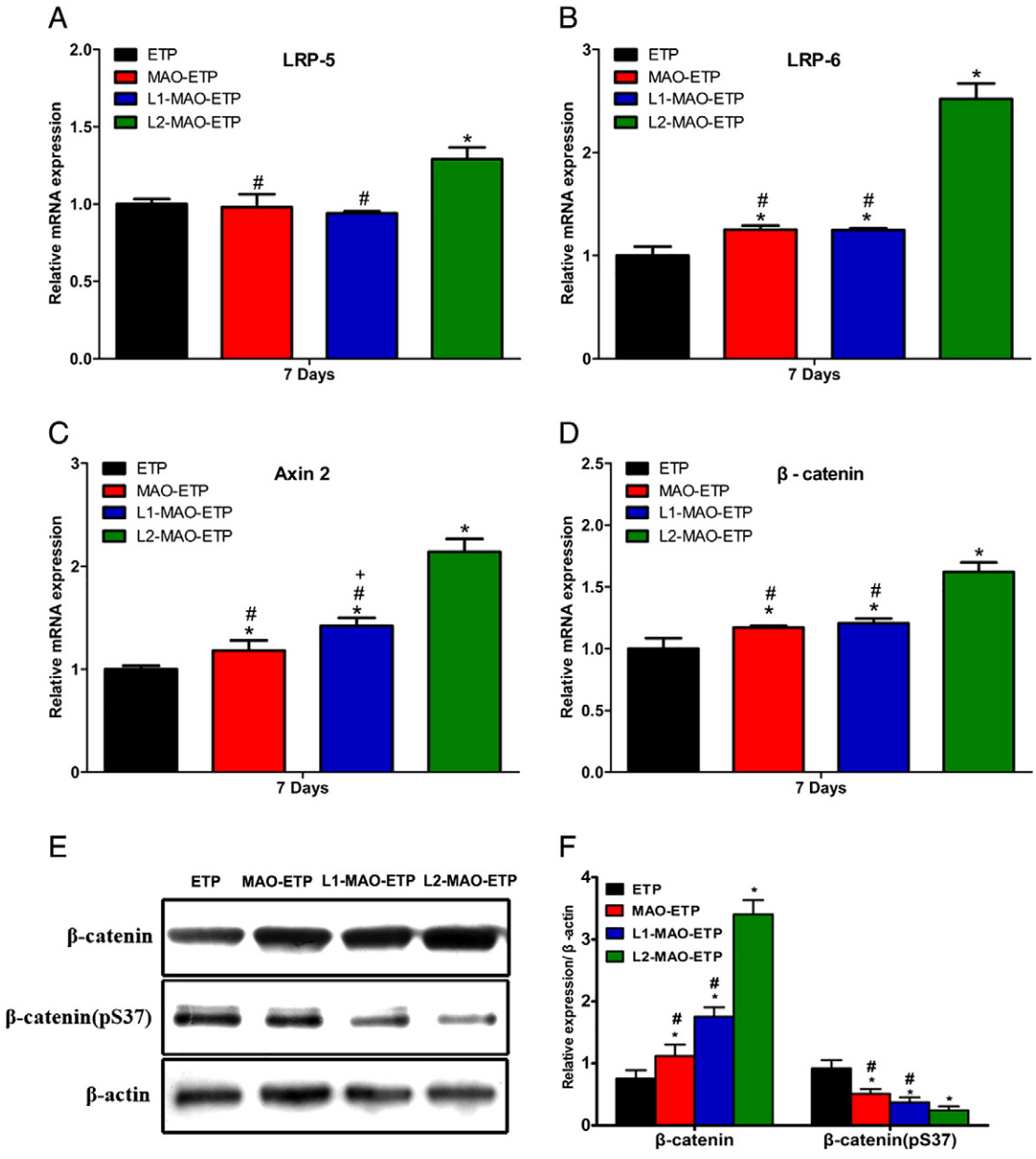

Figure 5. Wnt signal pathway related gene expression at day 7 for (**A**) LRP5, (**B**) LRP6, (**C**) Axin 2, (**D**) β-catenin, and (**E**) western blotting results of β-catenin and β-catenin (pS37). The symbols * and # represent $P < 0.05$ when compared with ETP and L2-MAO-ETP, respectively. A blank indicates no significant difference $P > 0.05$.

average maximum push-out loads obtained from the ETP, MAO-ETP, L1-MAO-ETP, and L2-MAO-ETP groups were 249.33 ± 35.30 N, 357.67 ± 26.65 N, 387.33 ± 31.56 N, and 473.00 ± 17.78 N, respectively. The ETP scaffold with MAO coatings (with or without Li) had a higher bonding strength than the uncoated ETP scaffold. In addition, the push-out load of the L1-MAO-ETP group was higher than that of the MAO-ETP group; however, there was no significant difference. The L2-MAO-ETP group contained a higher push-out load than that of the MAO-ETP and L1-MAO-ETP groups. Therefore, the higher Li content in the MAO coatings improved the interface osseointegration and new bone ingrowth.

Fluorescent microscopy of the sequential fluorochrome labels revealed the location and the dynamics of new bone formation in the various implants. After 4 weeks, the fluorescence of Alizarin Red S (red) was only present inside the marginal portion of the scaffold in the uncoated ETP group. For the MAO-ETP and L1-MAO-ETP groups, a widely spread area of Alizarin Red S fluorescence (red) was observed; however, it was not present in the center of the scaffolds. The fluorescence was shown in approximately all of the scaffold pores in the L2-MAO-ETP group (Figure 7). At 8 weeks, calcein (green) was incorporated into the bone closest to the titanium wires demonstrating similar patterns. Thus, the L2-ETP-MAO group showed the highest bone tissue growth.

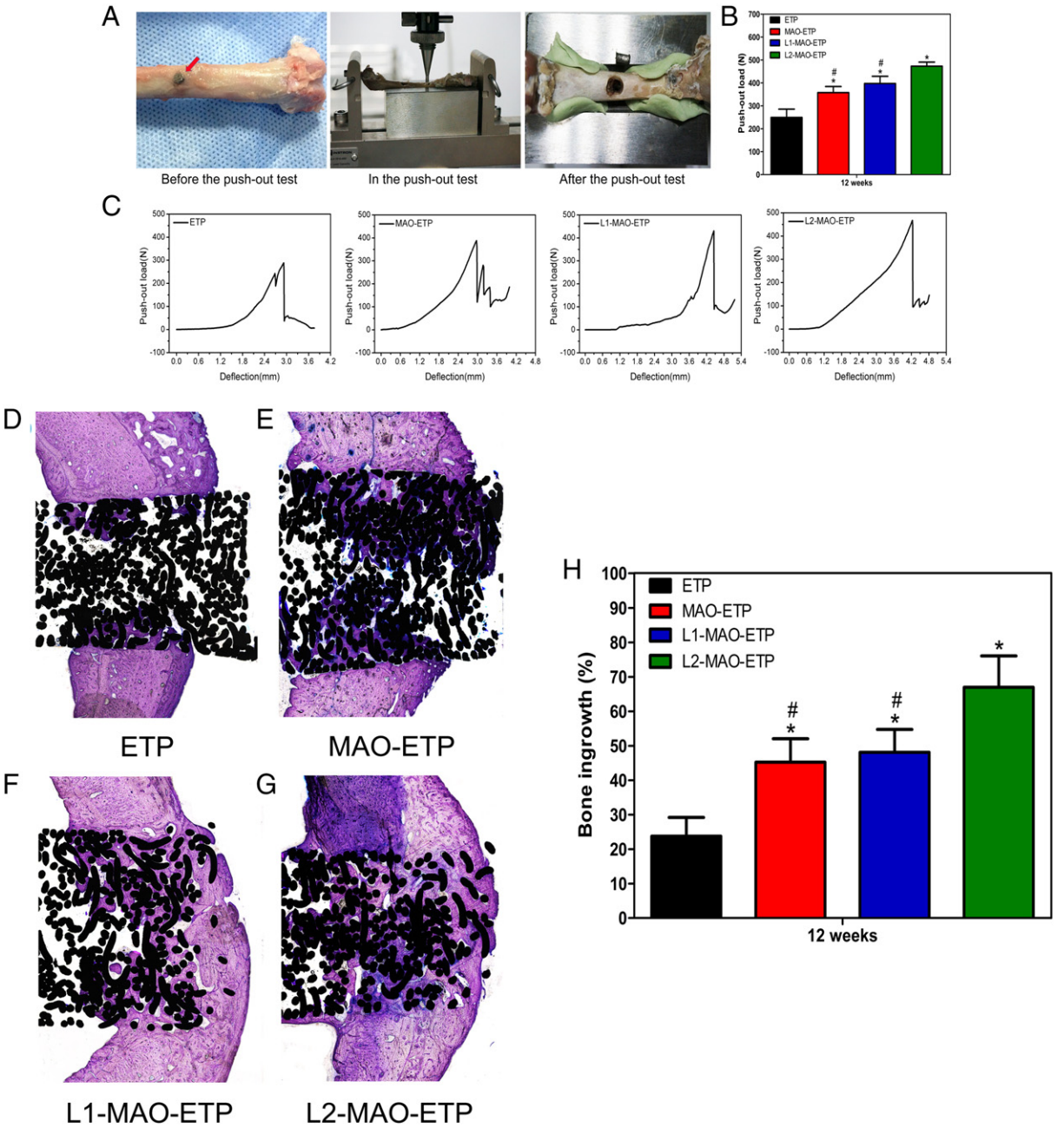

Figure 6. Push-out tests of the implants inserted in the femurs, toluidine blue staining of the sections, and percent of bone growth in the scaffolds. (A) Process of the push-out test, red arrow indicates implant. (**B**) Quantitative results of push-out test. (**C**) Typical load-deflection curves of push-out test. (**D**) ETP. (**E**) MAO-ETP. (**F**) L1-MAO-ETP. (**G**) L2-MAO-ETP. (**H**) Percent of bone ingrowth. (* and # represent $P < 0.05$ when compared with ETP and L2-MAO-ETP, respectively. A blank indicates no significant difference, $P > 0.05$.)

A histological analysis was performed to provide a detailed analysis on the new bone formation inside the pores of the scaffolds (Figure 6, *D-G*). In the uncoated ETP scaffold group, there was less bone formation around the periphery of the scaffolds, and the bone ingrowth was minimal. In the MAO-ETP and L1-MAO-ETP groups, more bone ingrowth was observed; however, some regions of the pores were not filled with bone. Furthermore, for the L2-MAO-ETP group, a larger amount of new bone grew into the interior of the scaffold, and approximately all pores were occupied by new bone. The bone ingrowth of the L2-MAO-ETP scaffold (66.98 ± 9.12%) was higher than those of the ETP (23.73 ± 5.47%, $p < 0.05$), MAO-ETP (45.22 ± 6.86%, $p < 0.05$), and L1-MAO-ETP (48.11 ± 6.68%, $p < 0.05$) scaffolds (Figure 6, *H*). Thus, the L2-MAO coatings promoted osteogenesis and osseointegration in vivo.

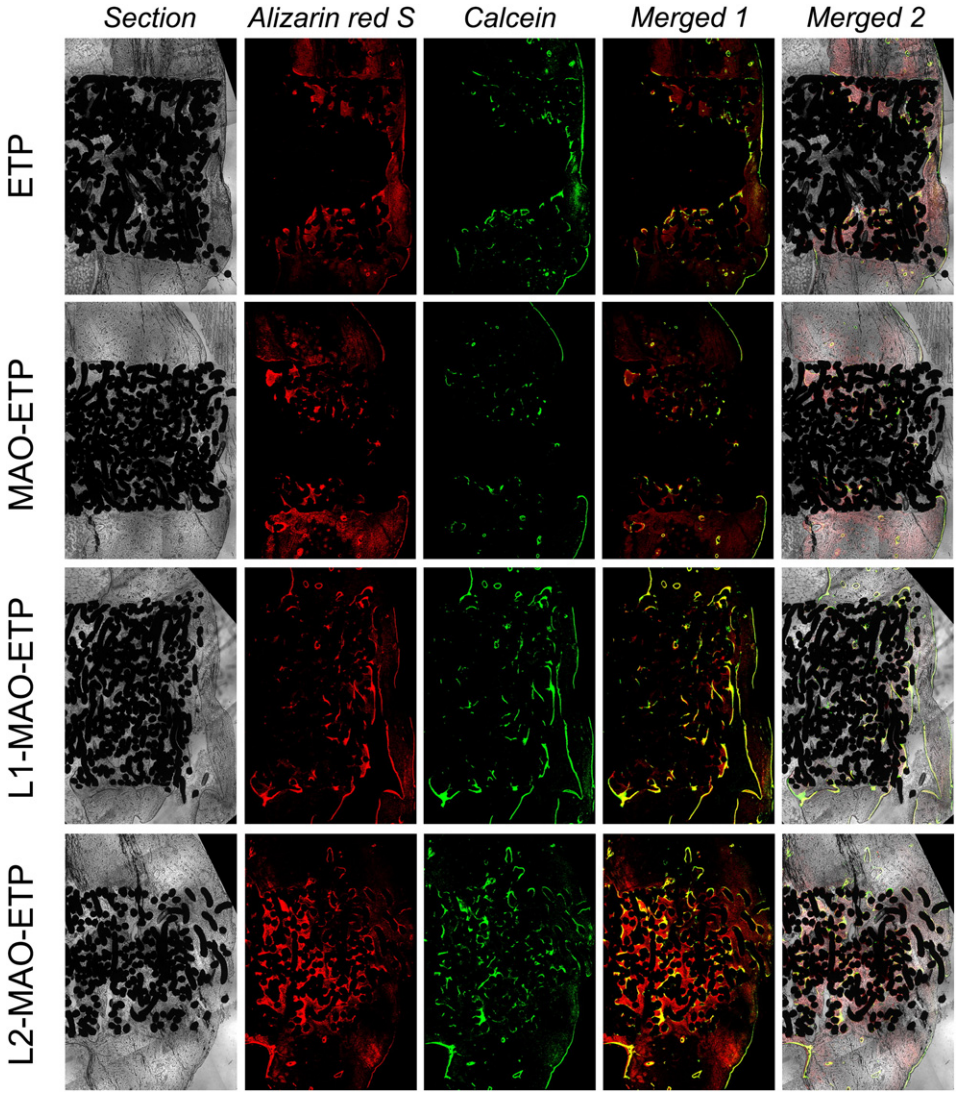

Figure 7. Sequential polychrome labeling of the new bone. The new bone was labeled with alizarin (red) and calcein (green).

Discussion

The activation of the Wnt/β-catenin signal transduction pathway has been reported to promote bone formation by affecting each step of the osteogenic process.[32] Based on the important role of the Wnt/catenin signal in osteogenesis (shown in Figure 8, *A*), Li and nano-porous coatings were simultaneously introduced on the surface of the ETP scaffold with MAO. Li was located on the coating, released to the surrounding microenvironment, then entered the cell through ion channels. Subsequently, Li stimulated the Wnt/β-catenin pathway by inhibiting the activity of GSK-3β and enhancing the concentration of β-catenin in the cytoplasm (Figure 8, *B*).[26] The MAO coating was designed to provide a nano-porous structure and to deliver Li to the implant sites. The hierarchical and compact coating on Li-MAO-ETP should be noticed. The micro-pores and hierarchical structure on the surface of the MAO titanium were beneficial for cell adhesion and proliferation.[33] Moreover, in this study, Li was incorporated into the coatings. Because the effect of the Li ion on cell proliferation and differentiation is dose dependent,[34] two MAO coatings with different amounts of Li on the surface of the ETP scaffold were prepared by adding 0.01 mol/L or 0.02 mol/L LiCl into the electrolytes. The ETP scaffolds with or without MAO coatings were used as controls. The stimulation effects and related mechanisms of the Li modified MAO coatings on the differentiation of MG63 in vitro were investigated, and then, an animal model was established to explore the effects of in vivo bone ingrowth.

The adhesion and spread of the anchorage-dependent cells on the surfaces were important for the cell division and growth.[35] In this study, the results of CLSM showed that well-developed actin filaments were apparent within the MG63 cells on the L2-MAO coatings. However, relatively sparse and diffuse actin filaments were observed within cells on the controls and L1-MAO coatings. Furthermore, SEM showed that the cells cultured on the L2-MAO coatings presented more filopodia extending to the edges. Thus, the metabolism and synthetic activity of the osteoblasts may be enhanced by the Li, which was also related

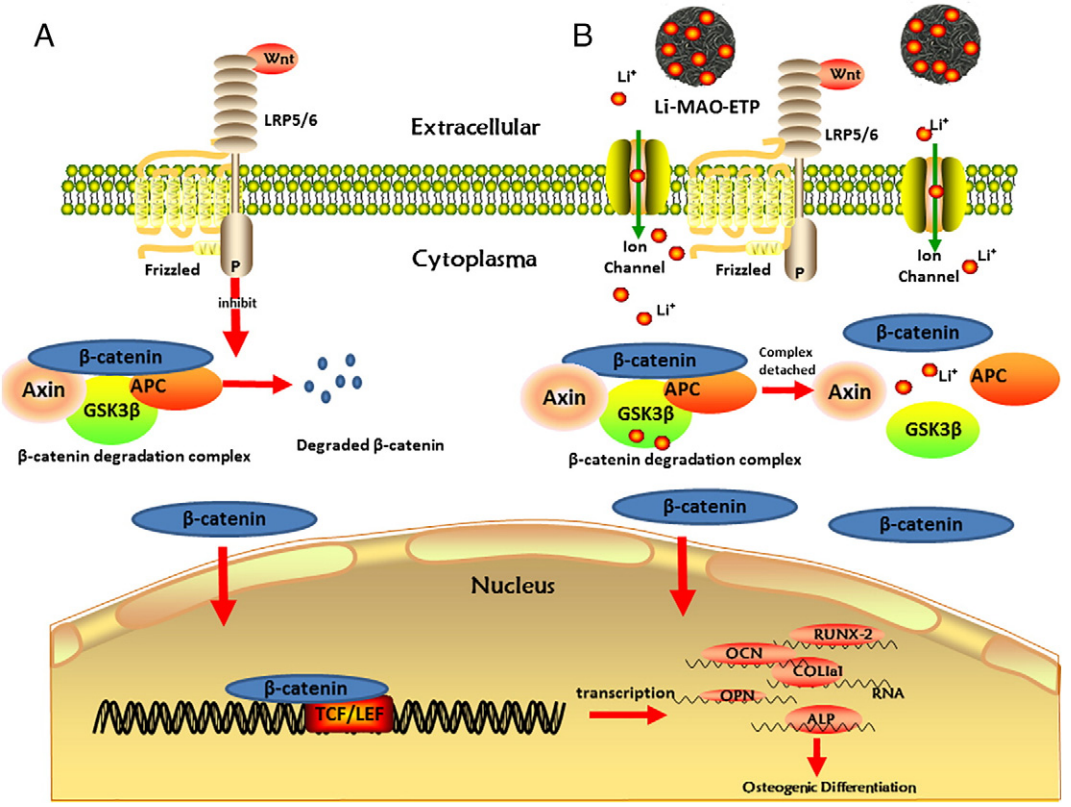

Figure 8. Mechanism of Li releasing from the Li-MAO-ETP scaffold in the activating Wnt signal pathway. (**A**) Canonical Wnt/β-catenin pathway in bone, (**B**) Li, released by the Li-MAO-ETP scaffold, in activating the Wnt signal pathway on bone differentiation.

with the amount of incorporated Li. The exiting Li localized on the surface and released to the surroundings enhanced the cell adhesion and spreading. In addition, the surface morphology changed by MAO may also favor cell adhesion. For the effects of the Li-incorporated MAO coating on cell proliferation and differentiation, the L2-MAO coatings enhanced MG-63 cell proliferation and early differentiation. Most importantly, the Runx2 mRNA expression of the MG63 cells on the L2-MAO coating was significantly higher than that on the controls. Runx2 is known to be an osteoblast-specific transcription factor that is essential for the differentiation of osteoblasts and can activate the expressions of downstream osteogenic genes, such as ALP, Col1a1, OC, and OPN.[36,37] In this study, the up-regulation of the early (Col1a1 and OPN), middle (ALP) and late (OC) osseo-specific markers of osteogenesis demonstrated that the L2-MAO coatings promoted the cell maturation and facilitated ECM mineralization at the early stage. For the L1-MAO coatings, although enhanced performances were observed, there was no significant difference when compared to the MAO coating.

The results of the in vivo experiments correlated with the above-mentioned in vitro results. The micro-CT evaluation, histological observations, and sequential fluorescent labeling demonstrated that the L2-MAO coatings could efficiently promote bone ingrowth, and approximately all pores were filled up with new bone. The push-out test revealed that the mechanical fixation of the L2-MAO-ETP scaffold was significantly stronger than the other scaffolds, thus confirming the enhanced osseointegration of the L2-MAO coatings. In general, a significant amount of Li was introduced into the MAO coatings thereby promoting the cell response in vitro and facilitating the bone formation in vivo. In addition, the degree of accelerated osteogenesis appeared to be associated with the Li content.

Recent studies have stated that the oral administration of Li stimulated the Wnt/β-catenin-mediated transcription in bone creating an increase in bone mass and an improvement in fracture healing.[26,27] In this study, our results also indicated similar results, and the Li-incorporated MAO coatings provided a steady release of Li ions into the surrounding growth medium. Therefore, the incorporation of Li into MAO coatings can stimulate the Wnt signal pathway, enhance cell proliferation and differentiation in vitro, and stimulate bone ingrowth in vivo.

The Wnt/β-catenin signal related gene expressions of LRP5, LRP6, Axin 2, and β-catenin were evaluated in this study. Lrp5, a co-receptor for the Wnt/b-catenin signal, regulates bone density. Early studies have shown that loss of function in Lrp5 could decrease the bone volume, formation rate, and osteoblast number. However, a gain of Lrp5 function could induce an increase in bone mass.[38–40] Axin is recognized as the most accurate reporter gene in the Wnt canonical pathway, since the association of the axin complex with the phosphorylated Lrp6 is believed to inhibit β-catenin phosphorylation and activate the β-catenin signal.[41] In this study, the up-regulation of LRP5, LRP6, Axin2, and β-catenin genes suggested that the Wnt/

β-catenin signal pathway could be activated by the L2-MAO coatings and thereby promote the cell response in vitro and enhance bone formation. Furthermore, the phosphorylated β-catenin protein levels were investigated by a western blot to verify that the incorporation of Li into the MAO coatings may inhibit the degradation of β-catenin in the cytoplasm. As estimated, the L2-MAO coatings significantly decreased the amount of phosphorylated β-catenin. Various studies have also demonstrated that Li ions or the Li-incorporated bioactive scaffolds could inhibit GSK3β activity, thereby allowing β-catenin to accumulate in the cytoplasm for Wnt pathway activation (Figure 8, *B*).[42,43] Therefore, we believed that incorporating a significant amount of Li into the MAO coatings could promote osteogenic proliferation and differentiation in vitro and in vivo through the Wnt/β-catenin pathway. In addition, the optimal amount of Li incorporated on the ETP scaffold requires further investigation.

Appendix A. Supplementary data

Supplementary data to this article can be found online at https://doi.org/10.1016/j.nano.2017.09.006.

References

1. Sen MK, Miclau T. Autologous iliac crest bone graft: should it still be the gold standard for treating nonunions? *Injury* 2007;**38**:S75-80.
2. Dimitriou R, Mataliotakis GI, Angoules AG, Kanakaris NK, Giannoudis PV. Complications following autologous bone graft harvesting from the iliac crest and using the RIA: a systematic review. *Injury* 2011;**42**:S3-S15.
3. Amin Yavari S, van der Stok J, Chai YC, Wauthle R, Tahmasebi Birgani Z, Habibovic P, et al. Bone regeneration performance of surface-treated porous titanium. *Biomaterials* 2014;**35**:6172-81, https://doi.org/10.1016/j.biomaterials.2014.04.054.
4. van der Stok J, Lozano D, Chai YC, Yavari SA, Coral APB, Verhaar JAN, et al. Osteostatin-coated porous titanium can improve early bone regeneration of cortical bone defects in rats. *Tissue Eng Part A* 2015;**21**:1495-506.
5. Dorozhkin SV. Bioceramics of calcium orthophosphates. *Biomaterials* 2010;**31**:1465-85.
6. He G, Liu P, Tan QB. Porous titanium materials with entangled wire structure for load-bearing biomedical applications. *J Mech Behav Biomed* 2012;**5**:16-31.
7. Liu P, Tan QB, Wu LH, He G. Compressive and pseudo-elastic hysteresis behavior of entangled titanium wire materials. *Mat Sci Eng A* 2010;**527**:3301-9.
8. Yan YY, Sun JF, Han Y, Li DC, Cui K. Microstructure and bioactivity of Ca, P and Sr doped TiO2 coating formed on porous titanium by micro-arc oxidation. *Surf Coat Technol* 2010;**205**:1702-13.
9. Terleeva OP, Sharkeev YP, Slonova AI, Mironov IV, Legostaeva EV, Khlusov IA, et al. Effect of microplasma modes and electrolyte composition on micro-arc oxidation coatings on titanium for medical applications. *Surf Coat Technol* 2010;**205**:1723-9.
10. Song WH, Jun YK, Han Y, Hong SH. Biomimetic apatite coatings on micro-arc oxidized titania. *Biomaterials* 2004;**25**:3341-9, https://doi.org/10.1016/j.biomaterials.2003.09.103.
11. Li LH, Kong YM, Kim HW, Kim YW, Kim HE, Heo SJ, et al. Improved biological performance of Ti implants due to surface modification by micro-arc oxidation. *Biomaterials* 2004;**25**:2867-75.
12. Li Y, Lee IS, Cui FZ, Choi SH. The biocompatibility of nanostructured calcium phosphate coated on micro-arc oxidized titanium. *Biomaterials* 2008;**29**:2025-32.
13. Matusiewicz H. Potential release of in vivo trace metals from metallic medical implants in the human body: from ions to nanoparticles—a systematic analytical review. *Acta Biomater* 2014;**10**:2379-403, https://doi.org/10.1016/j.actbio.2014.02.027.
14. Karner CM, Long F. Wnt signaling and cellular metabolism in osteoblasts. *Cell Mol Life Sci* 2016, https://doi.org/10.1007/s00018-016-2425-5.
15. MacDonald BT, Tamai K, He X. Wnt/β-catenin signaling: components, mechanisms, and diseases. *Dev Cell* 2009;**17**:9-26, https://doi.org/10.1016/j.devcel.2009.06.016.
16. Gaur T, Lengner CJ, Hovhannisyan H, Bhat RA, Bodine PVN, Komm BS, et al. Canonical WNT signaling promotes osteogenesis by directly stimulating Runx2 gene expression. *J Biol Chem* 2005;**280**:33132-40.
17. Galli C, Macaluso GM, Piemontese M, Passeri G. Titanium topography controls FoxO/beta-catenin signaling. *J Dent Res* 2011;**90**:360-4.
18. Yang F, Yang DZ, Tu J, Zheng QX, Cai LT, Wang LP. Strontium enhances osteogenic differentiation of mesenchymal stem cells and in vivo bone formation by activating wnt/catenin signaling. *Stem Cells* 2011;**29**:981-91.
19. Fromigue O, Hay E, Barbara A, Marie PJ. Essential role of nuclear factor of activated T Cells (NFAT)-mediated Wnt signaling in osteoblast differentiation induced by strontium ranelate. *J Biol Chem* 2010;**285**:25251-8.
20. Bain G, Muller T, Wang X, Papkoff J. Activated beta-catenin induces osteoblast differentiation of C3H10T1/2 cells and participates in BMP2 mediated signal transduction. *Biochem Biophys Res Commun* 2003;**301**:84-91.
21. Ma XY, Feng YF, Ma ZS, Li X, Wang J, Wang L, et al. The promotion of osteointegration under diabetic conditions using chitosan/hydroxyapatite composite coating on porous titanium surfaces. *Biomaterials* 2014;**35**:7259-70, https://doi.org/10.1016/j.biomaterials.2014.05.028.
22. Popelut A, Rooker SM, Leucht P, Medio M, Brunski JB, Helms JA. The acceleration of implant osseointegration by liposomal Wnt3a. *Biomaterials* 2010;**31**:9173-81.
23. Arioka M, Takahashi-Yanaga F, Sasaki M, Yoshihara T, Morimoto S, Hirata M, et al. Acceleration of bone regeneration by local application of lithium: Wnt signal-mediated osteoblastogenesis and Wnt signal-independent suppression of osteoclastogenesis (vol 90, pg 397, 2014). *Biochem Pharmacol* 2014;**91**:552-3.
24. Tang GH, Xu J, Chen RJ, Qian YF, Shen G. Lithium delivery enhances bone growth during midpalatal expansion. *J Dent Res* 2011;**90**:336-40.
25. Kugimiya F, Kawaguchi H, Ohba S, Kawamura N, Hirata M, Chikuda H, et al. GSK-3 beta controls osteogenesis through regulating Runx2 activity. *PLoS One* 2007;**2**.
26. Clement-Lacroix P, Ai MR, Morvan F, Roman-Roman S, Vayssiere B, Belleville C, et al. Lrp5-independent activation of Wnt signaling by lithium chloride increases bone formation and bone mass in mice. *Proc Natl Acad Sci U S A* 2005;**102**:17406-11.
27. Chen Y, Whetstone HC, Lin AC, Nadesan P, Wei QX, Poon R, et al. Beta-catenin signaling plays a disparate role in different phases of fracture repair: implications for therapy to improve bone healing. *PLoS Med* 2007;**4**:1216-29.
28. Schou M. Lithium treatment at 52. *J Affect Disord* 2001;**67**:21-32.
29. He G, Liu P, Tan Q. Porous titanium materials with entangled wire structure for load-bearing biomedical applications. *J Mech Behav Biomed Mater* 2012;**5**:16-31, https://doi.org/10.1016/j.jmbbm.2011.09.016.
30. Zhang W, Wang G, Liu Y, Zhao X, Zou D, Zhu C, et al. The synergistic effect of hierarchical micro/nano-topography and bioactive ions for enhanced osseointegration. *Biomaterials* 2013;**34**:3184-95, https://doi.org/10.1016/j.biomaterials.2013.01.008.
31. Wu J, Liu ZM, Zhao XH, Gao Y, Hu J, Gao B. Improved biological performance of microarc-oxidized low-modulus Ti-24Nb-4Zr-7.9Sn alloy. *J Biomed Mater Res B Appl Biomater* 2010;**92**:298-306, https://doi.org/10.1002/jbm.b.31515.

32. Manolagas SC, Almeida M. Gone with the Wnts: beta-catenin, T-cell factor, forkhead box O, and oxidative stress in age-dependent diseases of bone, lipid, and glucose metabolism. *Mol Endocrinol* 2007;**21**:2605-14.
33. Lincks J, Boyan BD, Blanchard CR, Lohmann CH, Liu Y, Cochran DL, et al. Response of MG63 osteoblast-like cells to titanium and titanium alloy is dependent on surface roughness and composition. *Biomaterials* 1998;**19**:2219-32.
34. Galli C, Piemontese M, Lumetti S, Manfredi E, Macaluso GM, Passeri G. GSK3b-inhibitor lithium chloride enhances activation of Wnt canonical signaling and osteoblast differentiation on hydrophilic titanium surfaces. *Clin Oral Implants Res* 2013;**24**:921-7.
35. Cheng MQ, Qiao YQ, Wang Q, Jin GD, Qin H, Zhao YC, et al. Calcium plasma implanted titanium surface with hierarchical microstructure for improving the bone formation. *ACS Appl Mater Interfaces* 2015;**7**:13053-61.
36. Tsigkou O, Jones JR, Polak JM, Stevens MM. Differentiation of fetal osteoblasts and formation of mineralized bone nodules by 45S5 Bioglass (R) conditioned medium in the absence of osteogenic supplements. *Biomaterials* 2009;**30**:3542-50.
37. Nayak S, Dey T, Naskar D, Kundu SC. The promotion of osseointegration of titanium surfaces by coating with silk protein sericin. *Biomaterials* 2013;**34**:2855-64.
38. Gong YQ, Slee RB, Fukai N, Rawadi G, Roman-Roman S, Reginato AM, et al. LDL receptor-related protein 5 (LRP5) affects bone accrual and eye development. *Cell* 2001;**107**:513-23.
39. Little RD, Carulli JP, Del Mastro RG, Dupuis J, Osborne M, Folz C, et al. A mutation in the LDL receptor-related protein 5 gene results in the autosomal dominant high-bone-mass trait. *Am J Hum Genet* 2002;**70**:11-9.
40. Holmen SL, Giambernardi TA, Zylstra CR, Buckner-Berghuis BD, Resau JH, Hess JF, et al. Decreased BMD and limb deformities in mice carrying mutations in both Lrp5 and Lrp6. *J Bone Miner Res* 2004;**19**:2033-40.
41. Zeng X, Huang H, Tamai K, Zhang XJ, Harada Y, Yokota C, et al. Initiation of Wnt signaling: control of Wnt coreceptor Lrp6 phosphorylation/activation via frizzled, dishevelled and axin functions. *Development* 2008;**135**:367-75.
42. Arioka M, Takahashi-Yanaga F, Sasaki M, Yoshihara T, Morimoto S, Hirata M, et al. Acceleration of bone regeneration by local application of lithium: Wnt signal-mediated osteoblastogenesis and Wnt signal-independent suppression of osteoclastogenesis. *Biochem Pharmacol* 2014;**90**:397-405.
43. Wu Y, Zhu SA, Wu CT, Lu P, Hu CC, Xiong S, et al. A Bi-lineage conducive scaffold for osteochondral defect regeneration. *Adv Funct Mater* 2014;**24**:4473-83.